中国激光

飞秒激光光丝空间特征的声学及荧光表征法：对比研究

荀明娜[1,2]，尚滨鹏[2,3]，齐鹏飞[2,3]，郭兰军[2,3*]，林列[2,4]，刘伟伟[2,3]

[1]北京大学物理学院人工微结构和介观物理国家重点实验室，北京 100871；

[2]南开大学现代光学研究所，天津 300350；

[3]天津市微尺度光学信息技术科学重点实验室，天津 300350；

[4]天津市光电传感器与传感网络重点实验室，天津 300350

摘要 飞秒激光成丝表征是光丝调控及应用的基础，成丝过程中光、声和热信号之间丰富的能量转换效应为利用声学和光学等方法探索和诊断光丝打开了大门。由于成丝过程中声波和荧光辐射微观物理机制的区别，两种信号与光丝物理参数之间的定量关系存在差异，然而目前仍缺乏两种方法的准确性对比研究。基于此，实验上通过研究脉冲能量对光丝空间分布的影响，系统对比了声学及荧光法两种光丝表征方法的异同。结果表明：两种方法都可以实现对光丝空间特征的表征，相比于荧光法，声学法对光丝起始和结束位置表现出更高的灵敏度，光丝内自由电子动能对光场强度的依赖性是造成差异的主要原因。

关键词 非线性光学；飞秒激光成丝；声学；荧光；空间特征；电子动能

中图分类号 O437 **文献标志码** A **DOI**：10.3788/CJL230434

1 引 言

高功率飞秒激光脉冲在空气中传输时，由于各种光学效应的综合作用，会发生自引导传输的物理现象，在传输过程中介质电离，产生均匀细长的等离子体通道，即光丝[1-4]。超快激光成丝处于超高激光强度、超快时间尺度、超远成丝距离以及多样化大气环境等极端的微观与宏观条件中[5-6]，在大气遥感探测[7-10]、激光雷达[11-12]、诱导云层放电[13-14]、太空垃圾清理[15]和超短强中红外-太赫兹脉冲产生[16-21]等领域中有着重大的应用前景。然而这些应用的前提和基础是对成丝过程的精准调控，这就迫切需要测量成丝过程中的激光参数、介质物理特性和光丝空间特征等[22]，从而为丰富实验认识、理解成丝机制及研究调控原理提供关键数据支持。

光丝内高强度的激光足以破坏任何探测器，这使得光丝的直接测量充满挑战[23-24]。然而成丝过程中光、声和热信号之间丰富的能量转换效应为探索和诊断光丝特性打开了大门。研究者提出了多种间接方法对光丝进行表征，并已经证明成丝过程中产生的声波及荧光是合适的可观测量，可以用于光丝的实验表征[25-26]。成丝过程中多光子电离产生的高能自由电子通过碰撞将能量转移给空气分子，空气受热膨胀导致冲击波发射，并很快衰减形成声波，声波的强度与光丝内的光场强度和自由电子密度紧密相关[27]。光丝内部分子的电离产生大量的高激发态正离子和中性分子，高能态粒子在向低能态跃迁的过程中辐射荧光[28]。由于荧光辐射是多光子电离的结果，因此荧光强度与光丝强度分布直接相关。研究表明，声学和荧光法是快速、无损的光丝表征方法，通过测量光轴不同位置处辐射的声信号和荧光信号，可以实时确定光丝的空间分布状态[29-31]。

上述研究一般采用声学法或荧光法某种单一的方法进行光丝表征，由于成丝过程中声波和荧光辐射微观物理机制的区别，两种信号与光丝物理参数之间的定量关系存在差异，然而目前仍缺乏两种方法的准确性对比研究。基于此，本文使用上述两种方法对空气中的飞秒激光光丝进行了多参数同步测量，并研究了单脉冲能量对光丝空间分布（起始位置、长度及强度分布等）的影响。物理机制的研究结果表明，光丝内自由电子动能对光场强度的依赖性是造成表征结果差异的主要原因。相比于荧光法，声学法对光丝的起始和结束位置表现出更高的测量灵敏度，更有利于弱光丝的实验表征。

2 实验装置

实验装置如图 1(a)所示。实验中使用了钛宝石飞秒脉冲激光器，输出脉冲激光中心波长为 800 nm，

收稿日期：2023-01-05；**修回日期**：2023-02-14；**录用日期**：2023-03-01；**网络首发日期**：2023-03-10

基金项目：国家重点研发计划(2018YFB0504400)、中央高校基本科研业务费专项资金(63223052)

通信作者：*guolanjun@nankai.edu.cn

脉宽为 50 fs，单脉冲能量为 5 mJ，重复频率为 500 Hz，光束直径为 8 mm，使用半波片和偏振分束器控制输入激光能量。飞秒激光束经过由平凹透镜 L1（焦距 $f=-75$ mm）和平凸透镜 L2（$f=500$ mm）组成的组合透镜后聚焦。通过改变 L1 和 L2 之间的相对距离，成丝位置可以在实验室允许范围内（<30 m）被精确控制，本实验中透镜组的几何焦距设置为 10 m。光丝诱导的声波和侧向 N_2 荧光信号的测量由入射激光脉冲触发。通过宽带麦克风（带宽为 4.5 MHz）在距离光丝 1 cm 的位置处检测光丝的声发射。此外，337 nm 处的 N_2 荧光被平凸透镜 L3（$f=50$ mm）收集到单色仪中并被连接在单色仪输出端的电压型光电倍增管（PMT）探测。来自麦克风的放大声信号与来自单色仪的 N_2 荧光信号同步显示在带宽为 300 MHz 的示波器上。麦克风与单色仪安装在同一位移台上并相对位于光丝的两侧，位移台平行于激光传播方向移动以检测光丝不同位置处激发的声信号和 N_2 荧光信号。实验中，以 2 cm 的位移间隔采集声波和荧光信号并对 256 次采集结果取平均以提高信噪比。实验测量的声波时域信号和 N_2 荧光光谱如图 1（b）、（c）所示，其中，图 1（c）插图所示为 PMT 输出的 337 nm 荧光时域信号，由于受到探测器和示波器响应时间和带宽的限制，信号下降时间远大于氮气荧光寿命（ns 量级）。

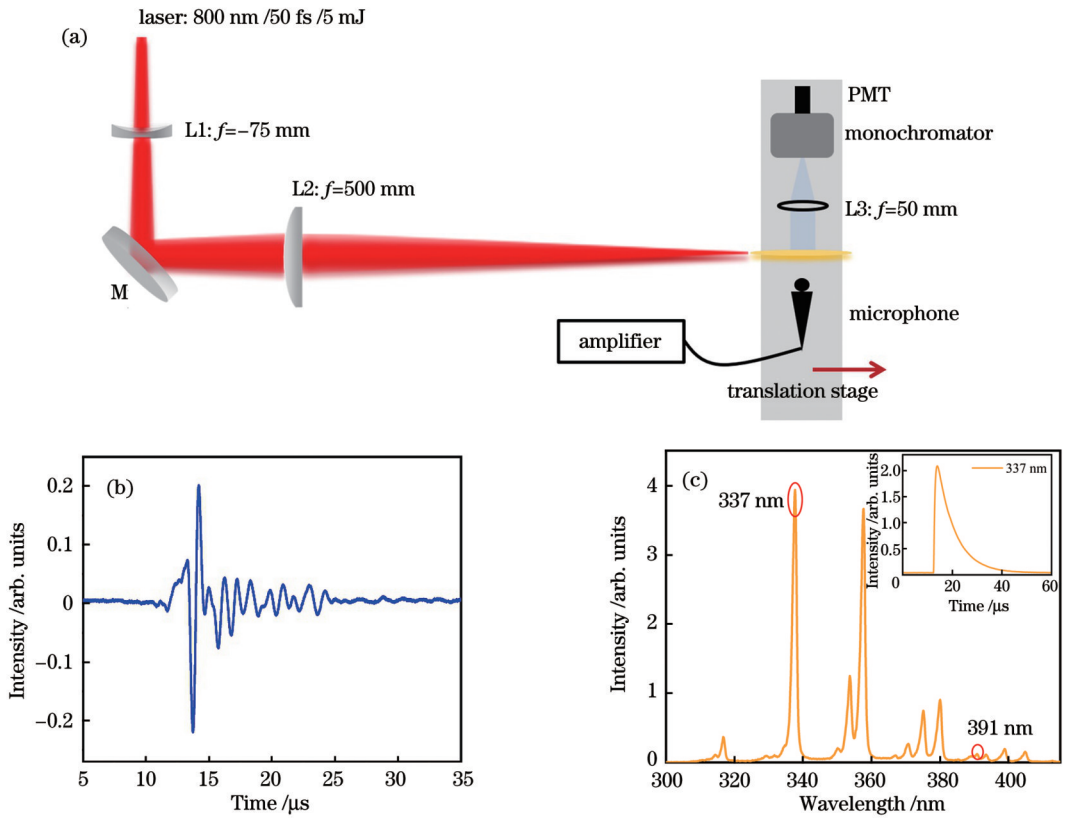

图 1　光丝诱导声波及荧光信号的测量。（a）实验装置示意图；（b）声波时域信号；（c）N_2 荧光光谱，插图为 PMT 探测得到的 337 nm 荧光时域信号

Fig. 1　Measurement of filament-induced acoustic wave and fluorescence signal. (a) Schematic of experimental facility; (b) acoustic time-domain signal; (c) N_2 fluorescence spectrum with 337 nm fluorescence time-domain signal detected by PMT shown in inset

3　实验结果与讨论

3.1　实验结果

为了标定两种探测方法的空间分辨率，使用了焦距为 $f=50$ mm 的透镜聚焦飞秒激光束以产生点源[图 2（a）插图]。图 2（a）、（b）分别为通过声学及荧光方法检测到的点源的空间分布。半峰全宽处（FWHM）的空间分辨率分别为 0.76 cm 和 0.84 cm，两种方法的空间分辨率相当。图 2（c）、（d）所示为焦距为 $f=10$ m 时声学及荧光法同步测量得到的光丝空间分布状态，脉冲能量恒定为 4.9 mJ，以实验环境中背景噪声的 3 倍标准差作为光丝出现的基准[32-34]。对比图 2（c）、（d）结果可知，声信号和荧光信号在整体上表现出一致的演化趋势：随着传输距离的增加，声信号和荧光信号都呈现先增加后减小的趋势。两种表征方法测量得到的信号峰位置都出现在 9.94 m 处，进一步表明两种方法都可以实现对光丝空间特征的表征，但是所得到的光丝起始和结束位置却存在显著差异。由图 2（c）可知，声学法测量获得的光丝起始和结束位置分别为 9.7 m 和 10.16 m，而荧光法测量获得的光丝起始和结束位置分

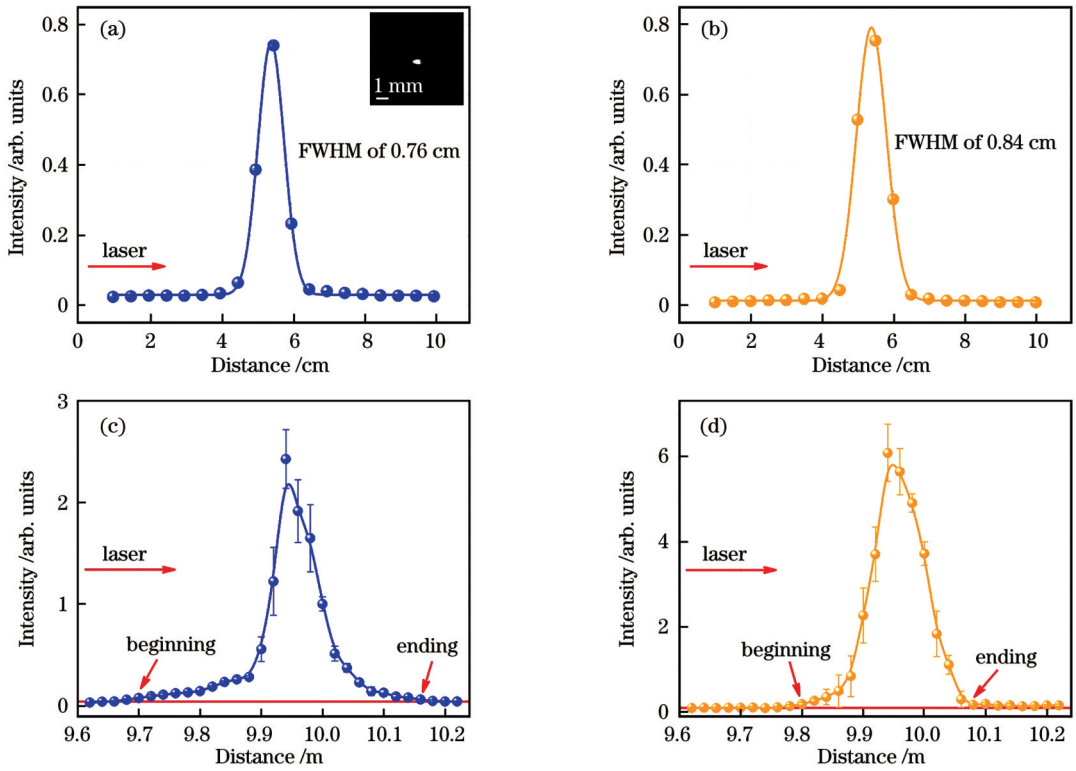

图 2　声学及荧光法的测量结果。当f=50 mm时点源诱导的(a)声信号强度(插图为点源图像)及(b)337 nm N_2荧光信号强度随激光传输距离的变化;当f=10 m,单脉冲能量为4.9 mJ时(c)声信号强度及(d)337 nm N_2荧光信号强度随激光传输距离的变化

Fig. 2　Measurement results by acoustic and fluorescent methods. (a) Acoustic signal intensity induced by point source (inset: image of point source) and (b) 337 nm N_2 fluorescence signal intensity versus propagation distance when f=50 mm; (c) acoustic signal intensity and (d) 337 nm N_2 fluorescence signal intensity versus propagation distance when f=10 m and single pulse energy is 4.9 mJ

别为9.8 m和10.08 m[图2(d)]。这使得声学方法测量得到的光丝长度大于荧光方法测量得到的光丝长度。

不同脉冲能量的飞秒激光脉冲聚焦形成的光丝诱导的声波强度及辐射的337 nm N_2荧光光谱强度的空间分布如图3(a)、(b)所示。可以看出,随着脉冲能量的增加,光丝的起始位置和峰值位置都逐渐靠近聚焦透镜L2,同时光丝的长度增加。这是因为随着脉冲能量的增加,空气的克尔自聚焦效应增强,激光光束的非线性克尔自聚焦位置靠近透镜位置,这使得成丝起始位置不断向聚焦透镜位置靠近,从而使得光丝长度随激光脉冲能量的增加而不断增大。

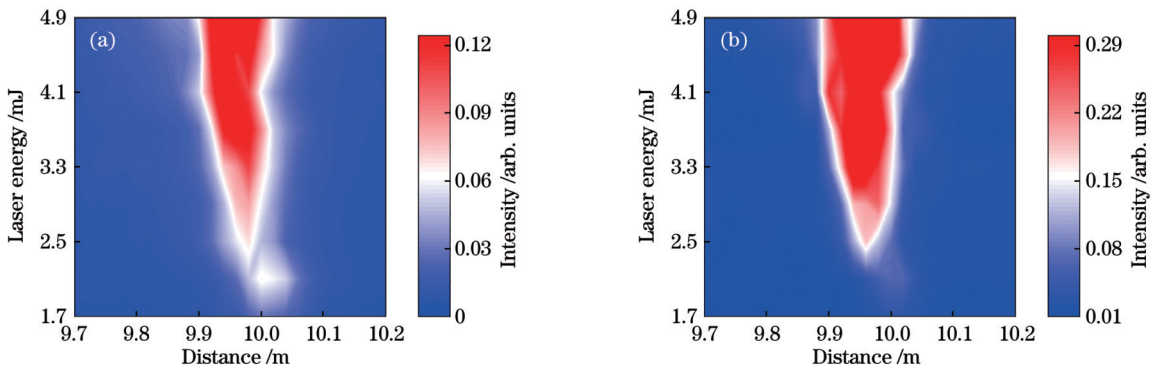

图 3　激光能量对光丝空间分布的影响。不同脉冲能量下光丝诱导的(a)声波强度及(b) 337 nm N_2荧光光谱强度的空间分布

Fig. 3　Effects of pulse energy on spatial distribution of filament. Spatial distributions of (a) acoustic signal intensity and (b) 337 nm N_2 fluorescence spectral intensity induced by filaments under different pulse energies

对比研究了两种方法测量得到的光丝起始位置和长度随脉冲能量的变化情况,实验结果如图4所示。相比于荧光法,声学法测量获得的光丝起始位置更靠近透镜L2,且光丝长度也更大,随着激光能量的增加,差异明显增大。当脉冲能量为1.7 mJ时,声学法测量获得的光丝起始位置和长度分别为9.9 m和0.24 m,

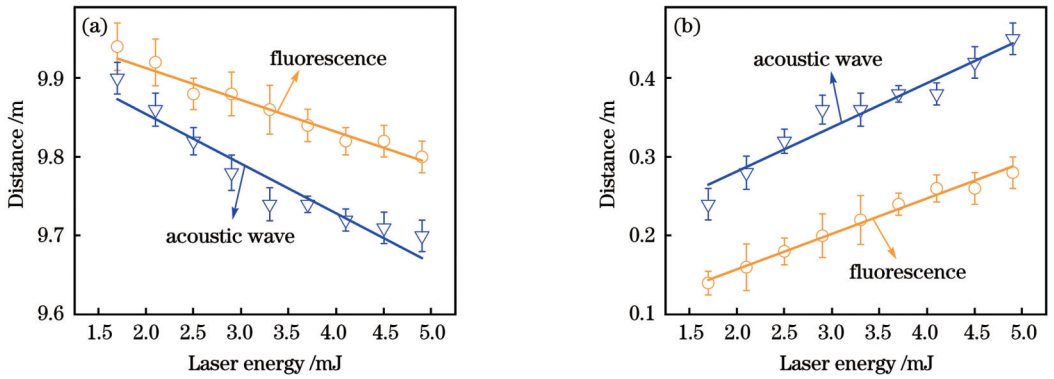

图 4　声学及荧光表征法的测量结果。光丝(a)起始位置及(b)长度随激光脉冲能量的变化

Fig. 4　Measurement results by acoustic and fluorescent characterization methods. (a) Starting position and (b) length of filament versus laser energy

荧光法测量获得的光丝起始位置和长度分别为 9.94 m 和 0.14 m，此时两种方法获得的起始位置和长度的差距分别为 0.04 m 和 0.1 m。而当单脉冲能量增加至 4.9 mJ 时，声学方法测量获得的光丝起始位置和长度分别为 9.7 m 和 0.46 m，而荧光方法测量获得的光丝起始位置和长度分别为 9.8 m 和 0.28 m，两种方法获得的起始位置和长度的差距分别为 0.1 m 和 0.18 m。

3.2　物理机制讨论

光丝内自由电子主要来自空气气体分子，在中心波长为 800 nm 的飞秒激光成丝过程中，电离产生的自由电子密度[35]可以表示为

$$\frac{\mathrm{d}N_e(t)}{\mathrm{d}t}=R_T\left[\frac{I(t)}{I_T}\right]^{\alpha}N(z),\tag{1}$$

式中：$N_e(t)$为电子密度；t为时间；$I(t)$为光丝内的激光强度；z为光丝传输距离；$N(z)$为脉冲传输方向上 z 处的中性分子密度；R_T和I_T为经验值；α为拟合系数。光丝内自由电子通过逆韧致辐射吸收激光能量，增加自身动能，其随时间的演化[36]可表示为

$$\frac{\mathrm{d}E_e(t)}{\mathrm{d}t}=k_1\frac{2e^2\nu_{\mathrm{eff}}}{m\omega^2\varepsilon_0 c}I(t)N_e(t),\tag{2}$$

式中：$E_e(t)$为电子动能；e为电子电荷；m为电子质量；ω为激光角频率；ε_0为真空介电常数；c为光速；ν_{eff}为电子和分子碰撞的有效频率；$k_1=\pi\varphi^2 l/4$，其中，φ为光丝直径，l为所测量的光丝长度。

研究表明，飞秒激光成丝时诱导的声波能量是电子吸收激光能量的一部分[37]，声信号[$s(t)$]与电子动能之间的关系可以表示为

$$s(t)=k_2\sqrt{E_e(t)},\tag{3}$$

式中：经验常数 $k_2=1.662\times10^6\ \mathrm{mV/J^{1/2}}$。电子通过非弹性碰撞将部分能量转移给周围的空气分子，导致空气体积快速膨胀，激发出等离子体冲击波，并很快衰变成声波。所测光丝任意位置 z 处声信号振幅的大小对应着该处电子动能的大小，进一步反映了光丝内的激光强度，因此声信号的大小随激光强度显著变化。

成丝时诱导的氮荧光主要来源于 N_2 的第二正带系 $C^3\Pi_u\rightarrow B^3\Pi_g$ 的跃迁和 N_2^+ 的第一负带系 $B^2\sum_u^+\rightarrow X^2\sum_g^+$ 的跃迁[38-41]。如图 1(c)所示，实验中观测到的 337 nm 和 391 nm 谱线分别由 N_2 和 N_2^+ 的激发产生。N_2^+ 的荧光发射机制已经被证实：强激光诱导的中性氮分子 σ_u2s 轨道的内层价电子发生多光子电离或者隧穿电离而形成 $N_2^+(B^2\sum_u^+)$，后经过 $B^2\sum_u^+\rightarrow X^2\sum_g^+$ 跃迁而辐射荧光。对于本实验中观测的 337 nm 荧光，通常是 N_2 与具有高动能的自由电子碰撞激发产生 $N_2(C^3\Pi_u)$，后经 $C^3\Pi_u\rightarrow B^3\Pi_g$ 跃迁而产生[42-43]：

$$N_2(X^1\sum_g^+)+e\rightarrow N_2(C^3\Pi_u)+e。\tag{4}$$

现有的研究表明：在 $1\times10^{13}\ \mathrm{W/cm^2}$ 光场强度下，电子获得的最大动能仅为 1.192 eV，这远远小于自由电子与 $N_2(X^1\sum_g^+)$ 碰撞产生激发态 $N_2(C^3\Pi_u)$ 所需的能量 11 eV[44]。而当飞秒激光强度增加到 $1.4\times10^{14}\ \mathrm{W/cm^2}$ 时，光丝内自由电子的能量将集中分布在 14.5 eV 左右，此时大量高动能电子将与基态氮分子发生碰撞并将其激发到 $N_2(C^3\Pi_u)$ 态，进而辐射 337 nm 荧光。

图 5(a)所示为声信号及 337 nm N_2 荧光信号强度随激光传输距离的归一化演化曲线。图 5(b)为声信号与荧光信号的相对偏差 $\delta=|I_a-I_f|/(I_a+I_f)$，其中 I_a 和 I_f 分别为声波和荧光信号的归一化强度。在 9.62～9.88 m 及 10.04～10.22 m 的传输范围内，相对偏差值都呈先增大后减小的趋势，而在 9.88～10.04 m 的传输范围内，相对偏差较小。因此飞秒激光成丝诱导声波及 337 nm 氮气荧光信号的物理过程如图 5 所示，该过程分为三个主要阶段。在成丝的初始和结束阶段即图 5 中Ⅰ、Ⅲ区域，较低的激光强度使得光丝内自由电子获得的动能较小，此时电子通过碰撞将能量转移给空气分子，造成空气体积的膨胀，进而诱导声波的产生，但是较低的电子动能不足以将 N_2 分子激发到激发态，因此实验中通常只能探测到微弱的声信号而无法检测到 337 nm N_2 荧光信号，这在图 5(b)中表现为两侧相

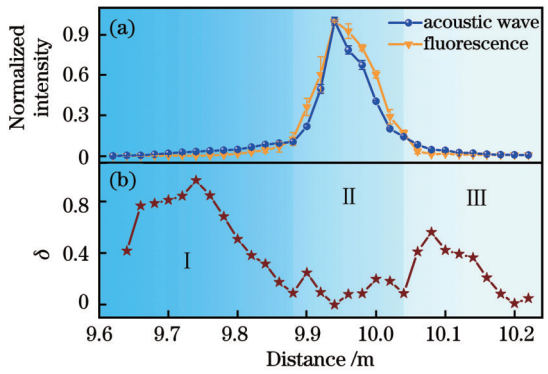

图 5 声学及荧光法测量结果的差异。(a)声信号及 337 nm N_2 荧光信号强度随激光传输距离的归一化演化曲线;(b)声波与荧光信号的相对偏差

Fig. 5 Differences in measurement results of acoustic and fluorescence methods. (a) Normalized evolution curves of acoustic signal intensity and 337 nm N_2 fluorescence signal intensity with laser transmission distance; (b) relative deviation between acoustic signal and fluorescent signal

对偏差较大,因此声学法测量得到的光丝长度大于荧光法测量得到的光丝长度。随着激光强度的增大,在强激光场作用下,光丝内自由电子获得较大的动能并通过碰撞将基态 N_2 分子激发到 $N_2(C^3\Pi_u)$ 态,后经 $C^3\Pi_u \rightarrow B^3\Pi_g$ 跃迁而辐射 337 nm 氮气荧光,此时相对偏差较小。随着激光强度的进一步增大,实验中可以同时检测到较强的声信号和 337 nm N_2 荧光信号,相对偏差值趋向于 0,如图 5 中Ⅱ区域所示。需要指出的是,沿激光传播方向,在远离光丝中心的两端位置,激光强度不足以电离空气发生成丝现象,声学和荧光信号辐射均接近于 0,此时测得的信号都表现为噪声水平,两者之间的偏差也逐渐归于 0。

4 结 论

使用声学及荧光法两种光丝表征方法对空气中的飞秒激光光丝进行了多参数同步测量,研究了单脉冲能量对光丝空间分布的影响。实验结果表明:随着脉冲能量的增加,光丝的起始位置和峰值位置同时向聚焦透镜方向移动,光丝长度增加,两种方法都可以实现对光丝空间特征的表征。相比于荧光法,声学法测量获得的光丝起始位置更靠近聚焦透镜且长度更大。物理机制的研究结果表明:光丝内自由电子动能对光场强度的依赖性是造成表征结果差异的主要原因,声学法对光丝的起始和结束位置表现出更高的灵敏度,更有利于弱光丝的实验表征。

参 考 文 献

[1] Bergé L, Skupin S, Nuter R, et al. Ultrashort filaments of light in weakly ionized, optically transparent media[J]. Reports on Progress in Physics, 2007, 70(10): 1633-1713.

[2] Couairon A, Mysyrowicz A. Femtosecond filamentation in transparent media[J]. Physics Reports, 2007, 441(2/3/4): 47-189.

[3] Kasparian J, Wolf J P. Physics and applications of atmospheric nonlinear optics and filamentation[J]. Optics Express, 2008, 16(1): 466-493.

[4] Wang X K, Ye J S, Sun W F, et al. Terahertz near-field microscopy based on an air-plasma dynamic aperture[J]. Light: Science & Applications, 2022, 11(1): 1-9.

[5] 刘伟伟, 薛嘉云, 苏强, 等. 超快激光成丝现象研究综述[J]. 中国激光, 2020, 47(5): 0500003.
Liu W W, Xue J Y, Su Q, et al. Research progress on ultrafast laser filamentation[J]. Chinese Journal of Lasers, 2020, 47(5): 0500003.

[6] Zang H W, Li H L, Zhang W, et al. Robust and ultralow-energy-threshold ignition of a lean mixture by an ultrashort-pulsed laser in the filamentation regime[J]. Light: Science & Applications, 2021, 10(1): 1-7.

[7] Rairoux P, Schillinger H, Niedermeier S, et al. Remote sensing of the atmosphere using ultrashort laser pulses[J]. Applied Physics B, 2000, 71(4): 573-580.

[8] Gravel J F, Luo Q, Boudreau D, et al. Sensing of halocarbons using femtosecond laser-induced fluorescence[J]. Analytical Chemistry, 2004, 76(16): 4799-4805.

[9] 解博夫, 赵星, 陶诗诗, 等. 自由曲面补偿飞秒激光成丝系统像差的应用研究[J]. 光学学报, 2023, 43(8): 0822055.
Xie B F, Zhao X, Tao S S, et al. Application of freeform surface in aberration compensation of femtosecond laser filamentation system[J]. Acta Optica Sinica, 2023, 43(8): 0822055.

[10] 王铁军, 陈娜, 郭豪, 等. 飞秒强激光大气遥感新技术的原理和研究进展[J]. 激光与光电子学进展, 2022, 59(7): 0700001.
Wang T J, Chen N, Guo H, et al. Principle and research progress of atmospheric remote sensing by intense femtosecond lasers[J]. Laser & Optoelectronics Progress, 2022, 59(7): 0700001.

[11] Kasparian J, Rodriguez M, Méjean G, et al. White-light filaments for atmospheric analysis[J]. Science, 2003, 301(5629): 61-64.

[12] Kosareva O, Panov N, Shipilo D, et al. Postfilament supercontinuum on 100 m path in air[J]. Optics Letters, 2021, 46(5): 1125-1128.

[13] Chin S L, Miyazaki K. A comment on lightning control using a femtosecond laser[J]. Japanese Journal of Applied Physics, 1999, 38(4R): 2011-2012.

[14] Pépin H, Comtois D, Vidal F, et al. Triggering and guiding high-voltage large-scale leader discharges with sub-joule ultrashort laser pulses[J]. Physics of Plasmas, 2001, 8(5): 2532-2539.

[15] Rubenchik A M, Fedoruk M P, Turitsyn S K. The effect of self-focusing on laser space-debris cleaning[J]. Light: Science & Applications, 2014, 3(4): e159.

[16] D'Amico C, Houard A, Franco M, et al. Conical forward THz emission from femtosecond-laser-beam filamentation in air[J]. Physical Review Letters, 2007, 98(23): 235002.

[17] Liu J L, Dai J M, Chin S L, et al. Broadband terahertz wave remote sensing using coherent manipulation of fluorescence from asymmetrically ionized gases[J]. Nature Photonics, 2010, 4(9): 627-631.

[18] Bai Y, Song L W, Xu R J, et al. Waveform-controlled terahertz radiation from the air filament produced by few-cycle laser pulses [J]. Physical Review Letters, 2012, 108(25): 255004.

[19] Fedorov V Y, Tzortzakis S. Powerful terahertz waves from long-wavelength infrared laser filaments[J]. Light, Science & Applications, 2020, 9(1): 186.

[20] Zhu X L, Weng S M, Chen M, et al. Efficient generation of relativistic near-single-cycle mid-infrared pulses in plasmas[J]. Light: Science & Applications, 2020, 9(1): 1-9.

[21] Kasparian J, Sauerbrey R, Chin S L. The critical laser intensity of self-guided light filaments in air[J]. Applied Physics B, 2000, 71(6): 877-879.

[22] 惠雨晨, 赵佳宇. 外电场作用下飞秒激光成丝辐射太赫兹波的全电流模型[J]. 光学学报, 2022, 42(1): 0114002.
Hui Y C, Zhao J Y. Full Current model for terahertz wave

generation from femtosecond laser filament under external electric fields[J]. Acta Optica Sinica, 2022, 42(1): 0114002.
[23] 郑恒毅, 尹富康, 王铁军, 等. 飞秒激光成丝的衍射分析方法[J]. 中国激光, 2022, 49(24): 2408001.
Zheng H Y, Yin F K, Wang T J, et al. Diffraction analysis of femtosecond laser filaments[J]. Chinese Journal of Lasers, 2022, 49(24): 2408001.
[24] Qi P F, Qian W Q, Guo L J, et al. Sensing with femtosecond laser filamentation[J]. Sensors, 2022, 22(18): 7076.
[25] Yu J, Mondelain D, Kasparian J, et al. Sonographic probing of laser filaments in air[J]. Applied Optics, 2003, 42(36): 7117-7120.
[26] Dubietis A, Tamosauskas G, Fibich G, et al. Multiple filamentation induced by input-beam ellipticity[J]. Optics Letters, 2004, 29(10): 1126-1128.
[27] Qin Q, Attenborough K. Characteristics and application of laser-generated acoustic shock waves in air[J]. Applied Acoustics, 2004, 65(4): 325-340.
[28] Waldenmaier T, Blümer J, Klages H. Spectral resolved measurement of the nitrogen fluorescence emissions in air induced by electrons[J]. Astroparticle Physics, 2008, 29(3): 205-222.
[29] Hosseini S A, Yu J, Luo Q, et al. Multi-parameter characterization of the longitudinal plasma profile of a filament: a comparative study[J]. Applied Physics B, 2004, 79(4): 519-523.
[30] Hao Z Q, Yu J, Zhang J, et al. Acoustic diagnostics of plasma channels induced by intense femtosecond laser pulses in air[J]. Chinese Physics Letters, 2005, 22(3): 636-639.
[31] Shang B P, Qi P F, Guo J W, et al. Manipulation of long-distance femtosecond laser filamentation: from physical model to acoustic diagnosis[J]. Optics & Laser Technology, 2023, 157: 108636.
[32] Guo J W, Sun L, Liu J P, et al. Beam wander restrained by nonlinearity of femtosecond laser filament in air[J]. Sensors, 2022, 22(13): 4995.
[33] Tao S S, Xie B F, Xue J Y, et al. Giant enhancement of acoustic and fluorescence emission from an off-axis reflective femtosecond laser filamentation system[J]. Optics Express, 2022, 30(21): 38745-38752.
[34] Xue J Y, Zhang N, et al. Effect of laser repetition rate on the fluorescence characteristic of a long-distance femtosecond laser filament[J]. Optics Letters, 2022, 47(21): 5676-5679.
[35] La Fontaine B, Vidal F, Comtois D, et al. The influence of electron density on the formation of streamers in electrical discharges triggered with ultrashort laser pulses[J]. IEEE Transactions on Plasma Science, 1999, 27(3): 688-700.
[36] Anglos D, Couris S, Fotakis C. Laser diagnostics of painted artworks: laser-induced breakdown spectroscopy in pigment identification[J]. Applied Spectroscopy, 1997, 51(7): 1025-1030.
[37] Colao F, Lazic V, Fantoni R, et al. A comparison of single and double pulse laser-induced breakdown spectroscopy of aluminum samples[J]. Spectrochimica Acta Part B: Atomic Spectroscopy, 2002, 57(7): 1167-1179.
[38] Danylo R, Zhang X, Fan Z Q, et al. Formation dynamics of excited neutral nitrogen molecules inside femtosecond laser filaments[J]. Physical Review Letters, 2019, 123(24): 243203.
[39] Lei M W, Wu C Y, Liang Q Q, et al. The fast decay of ionized nitrogen molecules in laser filamentation investigated by a picosecond streak camera[J]. Journal of Physics B: Atomic, Molecular and Optical Physics, 2017, 50(14): 145101.
[40] Li S Y, Li S C, Sui L Z, et al. Contribution of nitrogen atoms and ions to the luminescence emission during femotosecond filamentation in air[J]. Physical Review A, 2016, 93(1): 013405.
[41] Wang P, Xu S H, Li D H, et al. Spectroscopic study of laser-induced tunneling ionization of nitrogen molecules[J]. Physical Review A, 2014, 90(3): 033407.
[42] Mitryukovskiy S, Liu Y, Ding P J, et al. Plasma luminescence from femtosecond filaments in air: evidence for impact excitation with circularly polarized light pulses[J]. Physical Review Letters, 2015, 114(6): 063003.
[43] Itikawa Y. Cross sections for electron collisions with nitrogen molecules[J]. Journal of Physical & Chemical Reference Data, 2006, 35(1): 31-53.
[44] Wang Q J, Chen R, Zhang Y X, et al. Populations of $B_2\Sigma_u^+$ and $X_2\Sigma_g^+$ electronic states of molecular nitrogen ions in air determined by fluorescence measurement[J]. Physical Review A, 2021, 103(3): 033117.

Acoustic and Fluorescence Characterization of Femtosecond Laser Filament Spatial Properties: Comparative Study

Xun Mingna[1,2], Shang Binpeng[2,3], Qi Pengfei[2,3], Guo Lanjun[2,3*], Lin Lie[2,4], Liu Weiwei[2,3]

[1]*State Key Laboratory for Artificial Microstructure and Mesoscopic Physics, School of Physics, Peking University, Beijing* 100871, *China*;

[2]*Institute of Modern Optics, Nankai University, Tianjin* 300350, *China*;

[3]*Tianjin Key Laboratory of Micro-scale Optical Information Science and Technology, Tianjin* 300350, *China*;

[4]*Tianjin Key Laboratory of Optoelectronic Sensor and Sensing Network Technology, Tianjin* 300350, *China*

Abstract

Objective In recent years, femtosecond laser filamentation has attracted much attention and has shown great potential in atmospheric remote sensing owing to its unique characteristics. Femtosecond laser filamentation characterization is the basis of filament regulation and application. However, the high laser intensity and electron density in the plasma channel make it challenging to measure the filament directly. Fortunately, the energy conversion effects among light, acoustic, and thermal signals during filamentation enable studies into the exploration and diagnosis of filaments using acoustic and optical methods. Owing to difference in the microscopic physical mechanism of acoustic waves and fluorescence radiation during the filamentation process, there is a difference in the quantitative relationship between the two signals and the physical parameters of the filament. However, there is still a lack of comparative research on the accuracy of the two methods. This study investigates the effect of pulse energy on the spatial distribution of filament, and the differences and similarities between acoustic and fluorescence methods for characterizing filament are systematically compared. The reasons for the differences between the two methods are theoretically analyzed.

Methods The longitudinal plasma profile of filament induced by the propagation of an intense femtosecond laser pulse in air is measured simultaneously by employing acoustic and fluorescence methods. Acoustic emissions from the filament are detected by a directional microphone at a distance of 1 cm from the filament. To measure filament fluorescence, a convex lens (focal length $f=$ 50 mm) is employed to collect and focus the filament fluorescence onto the entrance slit of a monochromator. The dispersed fluorescence is detected by a photomultiplier tube placed at the exit slit of the monochromator. The triple standard deviation of the background noise is used as the reference for the appearance of the filament, and the differences and similarities between the acoustic and fluorescence methods in the spatial characterization of the filament are studied experimentally and theoretically.

Results and Discussions In order to calibrate the spatial resolution of the acoustic and fluorescence detection systems, the beam is focused by a single lens with 50 mm focal length to produce a point source. By measuring the spatial distribution of such a point source, it is determined that the spatial resolution of acoustic and fluorescent methods is 0.76 cm [Fig. 2(a)] and 0.84 cm [Fig. 2(b)], respectively, which are in agreement with the results reported previously (within one centimeter). The differences and similarities between acoustic and fluorescence methods in the spatial characterization of filament are compared and analyzed. Compared with the fluorescence method, the start position of the filament measured by the acoustic method is closer to the focusing lens and the length is larger [Figs. 2(c) and (d)]. This difference increases with an increase in filament length (Figs. 3 and 4). The analysis of the physical mechanism shows that the kinetic energy of free electrons in the filament is low owing to the low intensity of the light field at the start and end of the filament, which is much less than the kinetic energy (11 eV) of electrons needed to produce N_2 fluorescence through electron collision (Fig. 5).

Conclusions We present a simultaneous multi-parameter measurement on filament using acoustic and fluorescence methods, and the effect of pulse energy on the spatial distribution of the filament is studied. The experimental results show that the filament length increases with increasing laser energy. Simultaneously, the start and peak positions of the filament move toward the lens. Both methods can characterize the spatial characteristics of filaments. Compared with the fluorescence method, the start position of the filament measured by the acoustic method is closer to the focusing lens, and the length is larger. A study of the physical mechanism shows that the dependence of the free electron kinetic energy in the filament on the intensity of the light field is the main reason for the difference in the characterization results. The acoustic method shows higher sensitivity to the start and end positions of the filament, which is more conducive to the experimental characterization of the weak filament.

Key words nonlinear optics; femtosecond laser filamentation; acoustics; fluorescence; spatial characteristics; electron kinetic energy